Theoretical and Applied Fracture Mechanics 100 (2019) 281–288

Contents lists available at ScienceDirect

Theoretical and Applied Fracture Mechanics

journal homepage: www.elsevier.com/locate/tafmec

A comprehensive interpretation of the J-integral for cohesive interface cracks and interactions with matrix cracks

Johannes Scheel*, Andreas Ricoeur

University of Kassel, Institute of Mechanics, D-34125 Kassel, Mönchebergstraße 7, Germany

ARTICLE INFO

Keywords:
Crack tip loading
J-integral
Cohesive zones
Interface crack
Mixed-mode
Crack growth simulation

ABSTRACT

In linear elastic fracture mechanics various loading quantities exist to describe the crack tip loading, like stress intensity factors, the energy release rate or the J-integral. The J-integral is calculated along an arbitrary integration path and is related to the other loading quantities. In non-standard problems including e.g. temperature gradients, material inhomogeneities or interfaces, the path independence of the J-integral is only ensured considering additional terms. Material interfaces can be strong (perfect) or weak (imperfect), whereas dissipative processes only arise in weak interfaces. In this paper a matrix crack with a classical crack tip stress singularity is investigated, interacting with an interface crack, in the latter case modelling the fracture process zone in front of the physical crack tip by cohesive zone theory. The dissipation in the interface due to delamination has an influence on the loading of the matrix crack in terms of the J-integral and thus on its deflection and path. In order to identify this influence, the matrix crack tip loading is calculated accurately applying the J-integral in connection with a large integration contour enclosing the interface. Additional terms on the one hand ensure path independence, on the other their physical interpretation is desirable. In particular the contribution of the cohesive zone is considered closely, revealing a generalized mixed-mode relation of the J-integral and crack tip opening displacements, depending on the cohesive law, as in the classical mode I case, and on the boundary value problem. With multiple dissipative processes, the global energy release rate of the multi-crack system is not trivially calculated either. Numerical examples reveal e.g. that the matrix crack tip loading in the presence of an imperfect interface may be increased, even though energy is dissipated. Crack growth simulations show the preference of a matrix crack to grow into the direction of lower stiffness giving rise to an extremely attracting effect of damaged interfaces.

1. Introduction

The calculation of an accurate crack tip loading is necessary in order to safely evaluate whether a structure is at risk of fracture or to accurately predict paths of growing cracks. Both are becoming complex problems for heterogeneous, e.g. layered, structures or if any kind of inclusion is embedded in an otherwise homogenous matrix. Layers are connected and inclusions are bonded with the matrix at interfaces. These can be perfect or imperfect, whereas dissipative processes only arise in imperfect interfaces. The type, stiffness and possible damage evolution of the interface are having a crucial influence on cracks that might propagate in the matrix, as the matrix crack tip loading and thus the crack path are affected [1]. In order to predict the deflection of a growing matrix crack accurately, e.g. with the J-integral criterion [2], the relevant loading quantities also require accurate calculation. The path independent J-integral has proven to be an appropriate means to do so. It was introduced independently by Rice [3] and Cherepanov [4] and is related to the work of Eshelby [5] which characterizes generalized forces on dislocations and point defects in elastic fields. Rice [3] further correlated the J-integral with the Barenblatt type cohesive force model [6] for mode I loading conditions, enclosing the cohesive zone by an integration contour. First limited to straight cracks, the scalar J-integral was extended to the formulation of the J_k-integral vector by Budiansky and Rice [7], resulting in a path independent formulation for arbitrary crack geometries. Smelser and Gurtin [8] applied the J-integral to interface cracks, although focusing on the J_1 coordinate of the J_k-vector. They stated that the J-integral for bi-materials with a straight bonding line is equal to the original formulation for a homogenous body. An addition to that formulation is given by Khandelwal and Kishen [9], who also consider the J_2 coordinate. The matrix crack tip loading in the presence of a perfect interface has e.g. been given by Kuna [10]. All these works do not account for matrix crack tip loading

* Corresponding author.
E-mail addresses: j.scheel@uni-kassel.de (J. Scheel), ricoeur@uni-kassel.de (A. Ricoeur).

https://doi.org/10.1016/j.tafmec.2019.01.016
Received 7 December 2018; Received in revised form 14 January 2019; Accepted 21 January 2019
Available online 24 January 2019
0167-8442/

in the presence of an interface crack, in particular with fracture process zones modelled as cohesive zones. In order to calculate the J-integral in that case, sufficiently small integration contours around the matrix crack tip can be used, however bearing the difficulty of numerical inaccuracy and, considering crack growth simulations, preventing the matrix crack from growing sufficiently close to any kind of boundary. Therefore, remote integration contours are used to calculate the J-integral, requiring additional considerations to warrant path independence, where the interface crack tips are inevitably involved. In particular, physical interpretations of the integrals along the interface segments are sought within a fracture mechanical context. The relation to the total energy release rate will also be investigated. An interpretation of the contribution of the cohesive zone provides a generalized relation between the J-integral and the crack tip opening displacements (CTOD) for mixed mode conditions. In contrast to the classical single mode relation given in [3], CTOD and J-integral are not uniquely related by the cohesive law applied for mixed mode loading, where an additional term is introduced depending on the boundary value problem.

In numerical examples, the matrix crack tip loading in the presence of an imperfect interface is investigated with respect to the influence of interface parameters, interface shape and alignments of matrix and interface cracks. Crack growth simulations show the impact of interactions on crack paths, where a damaged interface proves to strongly attract a matrix crack even towards a stiffer region.

2. Derivations and discussions of the J-integral and the energy release rate

In the following, the J-integral of a matrix crack will be derived in the presence of either a cohesive interface edge or center crack. The latter contributions will be further investigated separately seeking a physical interpretation with respect to energy dissipation and cohesive zone theory. Furthermore, the global energy release rate is derived. As a third case, being relevant for applications and the numerical examples, a self-contained interface of an inclusion is considered.

2.1. Matrix crack and interface edge crack

A matrix crack in a bi-material body consisting of regions A and B separated by an interface is depicted in Fig. 1(a). The interface is separated into three parts: a closed section Γ_I^{closed}, a cohesive zone Γ_I^{coh} and free surfaces Γ_I^{open}. The matrix crack tip loading in terms of the J-integral vector, using an infinitely small integration contour Γ_ϵ, is defined as

$$J_k = \lim_{\epsilon\to 0} \int_{\Gamma_\epsilon} Q_{kj} n_j \mathrm{d}\Gamma, \tag{1}$$

where n_j is the unit outward normal on Γ_ϵ and Eshelby's energy momentum tensor is introduced as $Q_{kj} = u\delta_{kj} - \sigma_{ij} u_{i,k}$, where u is the potential energy density, δ_{ij} the identity tensor, σ_{ij} the stress tensor and $u_{i,k}$ the displacement gradient. The index notation is used for tensor operations, implying summation over repeated indices holding values one and two. The calculation with a remote integration contour Γ (Fig. 1(a)) enclosing the interface needs further investigation. The contour is split into sub-contours, yielding opposing orientations of the integral paths along the interface with unit normals $n_j^A = -n_j^B$ and continuous tractions $t_i^A = -t_i^B = t_i$. The superscripts A/B indicate affiliations of the quantities to subdomains A or B. The J-integral vector of the matrix crack reads

$$\begin{aligned} J_k = \lim_{\epsilon\to 0} & \int_{\Gamma^+} (u^+ - u^-) n_k^+ \mathrm{d}\Gamma + \int_{\Gamma_A} Q_{kj}^A n_j \mathrm{d}\Gamma + \int_{\Gamma_B} Q_{kj}^B n_j \mathrm{d}\Gamma \\ & + \int_{\Gamma_{IB}^{closed}} (Q_{kj}^B - Q_{kj}^A) n_j^B \mathrm{d}\Gamma \quad + \int_{\Gamma_{IB}^{open}} (u^B - u^A) n_k^B \mathrm{d}\Gamma \\ & + \underbrace{\int_{\Gamma_{IB}^{coh}} (Q_{kj}^B - Q_{kj}^A) n_j^B \mathrm{d}\Gamma}_{-J_k^{coh}}. \end{aligned} \tag{2}$$

Γ^+/Γ^- represent the matrix crack surfaces, for which the accurate calculation holds its own challenges, particularly close to the crack tip. A comprehensive description is beyond the scope of this paper and has been discussed by Eischen [11] or more recently by Judt and Ricoeur [12]. Γ_{IB}^{open} describes further free surfaces, again being traction free, leaving the jump of potential energy to integrate. Γ_{IB}^{closed} describes the perfectly closed part of the interface. The integrand is a jump of the energy momentum tensor, more precisely described e.g. by Kuna [10]. It vanishes for equal materials $A = B$. For the contour describing the cohesive zone Γ_{IB}^{coh}, the integrand also is a jump of the energy momentum tensor. The corresponding integral

$$\begin{aligned} J_k^{coh} &= -\int_{\Gamma_{IB}^{coh}} \{(u^B - u^A) n_k^B - (u_{i,k}^B - u_{i,k}^A) t_i^B\} \mathrm{d}\Gamma \\ &= -\int_{\Gamma_{IB}^{coh}} \{(u^B - u^A) n_k^B + (u_i^B - u_i^A)_{,k} t_i\Big\} \mathrm{d}\Gamma \\ &= -\int_{\Gamma_{IB}^{coh}} \{(u^B - u^A) n_k^B + \delta_{i,k} t_i\Big\} \mathrm{d}\Gamma, \end{aligned} \tag{3}$$

will now be investigated. The partitioned J-integral vector of the cohesive zone is thus composed of a jump of the potential energy and the scalar product of the gradient of interface separation $\delta_{i,k}$ and the traction vector t_i. δ_i is generally defined as the interface separation and, looking at the explicit example of Fig. 1(a) and introducing a local coordinate system x_1^*, x_2^*, gives $\delta_i(x_1^*, 0) = u_i^B(x_1^*, 0) - u_i^A(x_1^*, 0) = \delta_i(x_1^*)$. By simple substitution and with $\delta_i(l_1) = \delta_i^t$ and $\delta_i(l_2) = 0$ the first coordinate of Eq. (3) turns into

$$\begin{aligned} J_1^{*coh} &= -\int_{\Gamma_{IB}^{coh}} \delta_{i,1}(x_1^*) t_i \mathrm{d}\Gamma = -\int_{l_1}^{l_2} \frac{d\delta_1(x_1^*)}{dx_1^*} t_1 \mathrm{d}x_1^* - \int_{l_1}^{l_2} \frac{d\delta_2(x_1^*)}{dx_1^*} t_2 \mathrm{d}x_1^* \\ &= \int_0^{\delta_1^t} t_1 \mathrm{d}\delta_1 + \int_0^{\delta_2^t} t_2 \mathrm{d}\delta_2 = +J_{1,II}^{*coh} + J_{1,I}^{*coh}, \end{aligned} \tag{4}$$

assuming that the tractions are only functions of the mode-associated separations, i.e. $t_i = f(\delta_i(x_1^*)) = f(x_1^*)$. Here, $\delta_i^t = \delta_{1/2}^t$ describe the opening separations at the physical crack tip and $J_{1,I/II}^{*coh}$ describe the areas underneath the traction-separation curves in the interval $[0, \delta_i^t]$ and the dissipated surface energy density in case of crack growth, i.e. $\delta_i^t = \delta_{ic}^t$, with a critical separation δ_{ic}^t. The second coordinate of J_k^{coh} needs further investigation as the separation gradient $\delta_{i,k}$ with respect to x_2^* is not zero in spite of $\delta_i(x_1^*)$. Therefore the second coordinate of J_k^{coh} is introduced as

$$\begin{aligned} J_2^{*coh} &= -\lim_{x_2^{*B/A}\to 0} \int_{l_1}^{l_2} \{(u^B - u^A) n_2^B \\ &\quad + (u_i^B(x_1^*, x_2^{*B}) - u_i^A(x_1^*, x_2^{*A}))_{,2} t_i\} \mathrm{d}x_1^* \\ &= -\int_{l_1}^{l_2} (u^B - u^A) n_2^B \mathrm{d}x_1^* - \lim_{x_2^{*B/A}\to 0} \int_{l_1}^{l_2} \frac{\partial \tilde{\delta}_1(x_1^*, x_2^{*B/A})}{\partial x_2^*} t_1 \mathrm{d}x_1^* \\ &\quad - \lim_{x_2^{*B/A}\to 0} \int_{l_1}^{l_2} \frac{\partial \tilde{\delta}_2(x_1^*, x_2^{*B/A})}{\partial x_2^*} t_2 \mathrm{d}x_1^*, \end{aligned} \tag{5}$$

where $\tilde{\delta}_i(x_1^*, x_2^{*B/A})$ is the separation between two arbitrary points in the subdomains A and B. With that the derivative is nonzero and the limit of $x_2^{*B/A} \to 0$ needs to be considered in order to obtain values at the interface. In Eq. (5) a simple substitution as in Eq. (4) is not possible, so that the second coordinate J_2^{*coh} cannot be related to the physical crack tip opening separations δ_i^t. Thus, the first row of Eq. (5) is elaborated, inserting the potential energy density $u = \sigma_{ij}\varepsilon_{ij}/2$ and taking into account that σ_{22} is continuous at the interface:

$$J_2^{*coh} = \frac{1}{2} \int_{l_1}^{l_2} [\sigma_{11}^B \varepsilon_{11}^B - \sigma_{11}^A \varepsilon_{11}^A + (\varepsilon_{22}^A - \varepsilon_{22}^B)\sigma_{22}] \mathrm{d}x_1^*. \tag{6}$$

For the chosen coordinate system $n_2^B = -1$ holds for the interface unit normal. The tangential strain $\varepsilon_{11}^{A/B}$ is only continuous for perfectly bonded interfaces and thus has to remain separated in Eq. (6). With Eqs. (4) and (6), and the first coordinate of the interface unit normal in the chosen coordinate system being $n_1^B = 0$, J_k^{coh} of Eq. (3) yields

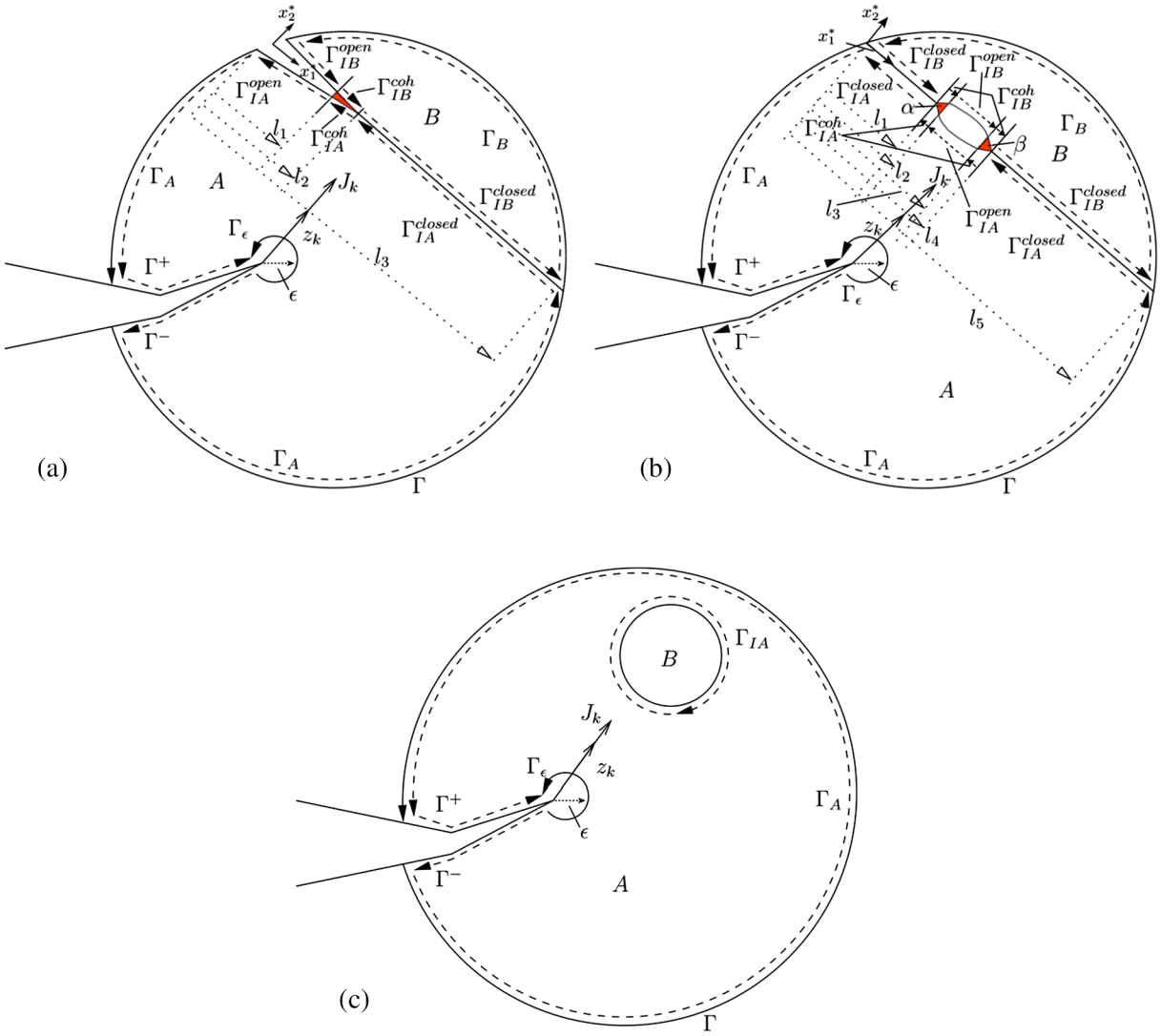

Fig. 1. Remote and near tip integration contours for the J_k-integral of the matrix crack tip in the presence of a cohesive interface edge (a) or center (b) crack and a self-contained interface (c).

$$J_k^{coh}\vec{e}_k^{*} = (J_{1,I}^{*coh} + J_{1,II}^{*coh})\vec{e}_1^{*} + \frac{1}{2}\int_{l_1}^{l_2}[\sigma_{11}^B\varepsilon_{11}^B - \sigma_{11}^A\varepsilon_{11}^A + (\varepsilon_{22}^A - \varepsilon_{22}^B)\sigma_{22}]\mathrm{d}x_1^{*}\vec{e}_2^{*}. \tag{7}$$

Eq. (7) gives evidence that for the cohesive crack under mixed mode loading, the J-integral vector has two nonzero coordinates, being the mixed mode extension to the single mode formulation given by Rice [3]. Whereas the mixed mode generalization in J_1 is straightforward, J_2 exhibits jump terms which are zero for pure mode-I/II loadings. It is remarkable that just J_1 is uniquely related to the CTOD δ_i^t by the cohesive laws $t_i(\delta_i)$, whereas J_2 emanates from tangential and normal stress and strain at the faces of the cohesive zone, thus depending on the boundary value problem.

By inserting Eq. (7), the matrix crack tip loading of Eq. (2) becomes

$$\begin{aligned} J_k\vec{e}_k^{*} &= \lim_{\epsilon\to 0}\int_{\Gamma_\epsilon} Q_{kj}n_j\mathrm{d}\Gamma\vec{e}_k^{*} \\ &= \{\lim_{\epsilon\to 0}\int_{\Gamma^+}(u^+ - u^-)n_k^+\mathrm{d}\Gamma + \int_{\Gamma_A} Q_{kj}^A n_j\mathrm{d}\Gamma + \int_{\Gamma_B} Q_{kj}^B n_j\mathrm{d}\Gamma \\ &+ \int_{l_2}^{l_3}(Q_{k2}^A - Q_{k2}^B)\mathrm{d}x_1^{*}\}\vec{e}_k^{*} + \int_0^{l_1}(u^A - u^B)\mathrm{d}x_1^{*}\vec{e}_2^{*} \\ &- (J_{1,I}^{*coh} + J_{1,II}^{*coh})\vec{e}_1^{*} + \tfrac{1}{2}\int_{l_1}^{l_2}[\sigma_{11}^A\varepsilon_{11}^A - \sigma_{11}^B\varepsilon_{11}^B + (\varepsilon_{22}^B - \varepsilon_{22}^A)\sigma_{22}]\mathrm{d}x_1^{*}\vec{e}_2^{*}, \end{aligned} \tag{8}$$

explicitly exhibiting a jump of potential energy in $[0, l_1]$ and $[l_2, l_3]$, as $Q_{k2}^A - Q_{k2}^B$ also includes an energy jump.

Being able to calculate the matrix crack tip loading in terms of the J-integral vector using remote integration contours and physically understanding the additional integral constituents ensuring path independence, the global energy release rate of the system is considered next. It is introduced as the sum of the energy release rates of all single crack tips [13]

$$\hat{G} = \sum_{n=1}^{N} G^{(n)} = \sum_{n=1}^{N} J_k^{(n)} z_k^{(n)}, \tag{9}$$

where N is the total number of crack tips in the system and $z_k^{(n)}$ are the unit vectors of crack growth. Applying Eq. (9) to the system of Fig. 1(a) leads to:

$$\begin{aligned} \hat{G} = J^{matrix} + J^{coh} &= J_k z_k + J_k^{coh} z_k^{coh} = \left(\lim_{\epsilon\to 0}\int_{\Gamma_\epsilon} Q_{kj}n_j\mathrm{d}\Gamma\right)z_k \\ &+ \left(\lim_{\epsilon\to 0}\int_{\Gamma^{coh}} Q_{kj}n_j\mathrm{d}\Gamma\right)z_k^{coh}. \end{aligned} \tag{10}$$

The J-integral vectors could thus be calculated with small integration contours. For the matrix crack the contour is depicted in Fig. 1(a) and for the interface crack a counter clockwise integration contour $\Gamma^{coh} = -\Gamma_{IA}^{coh} - \Gamma_{IB}^{coh}$ is shrunk to the cohesive surfaces. In the chosen coordinate system x_1^{*}, x_2^{*}, the vector of cohesive crack growth is

$z_k^{coh} \triangleq \vec{e}_1^*$, so that the J-integral of the cohesive crack according to Eq. (7) is related to the energy release rates of the applied loading modes as follows:

$$J^{coh} = J_k^{coh} z_k^{coh} = J_{1,I}^{*coh} + J_{1,II}^{*coh} = G^{coh} = G_I^{coh} + G_{II}^{coh}. \tag{11}$$

With this relation and keeping in mind that remote integration contours (see e.g. Eq. (8)) are beneficial, the total energy release rate results in

$$\begin{aligned}\hat{G} = (&\left\{\lim_{\epsilon\to 0}\int_{\Gamma^+}(u^+ - u^-)n_k^+ \mathrm{d}\Gamma + \int_{\Gamma_A} Q_{kj}^A n_j \mathrm{d}\Gamma\right.\\ &\left. + \int_{\Gamma_B} Q_{kj}^B n_j \mathrm{d}\Gamma + \int_{l_2}^{l_3}(Q_{k2}^A - Q_{k2}^B)\mathrm{d}x_1^*\right\}\vec{e}_k^*\\ &+ \int_0^{l_1}(u^A - u^B)\mathrm{d}x_1^*\vec{e}_2^* - (J_{1,I}^{*coh} + J_{1,II}^{*coh})\vec{e}_1^*\\ &+ \frac{1}{2}\int_{l_1}^{l_2}[\sigma_{11}^A\varepsilon_{11}^A - \sigma_{11}^B\varepsilon_{11}^B + (\varepsilon_{22}^B - \varepsilon_{22}^A)\sigma_{22}]\mathrm{d}x_1^*\vec{e}_2^*\Big)z_k\\ &+ G_I^{coh} + G_{II}^{coh}.\end{aligned} \tag{12}$$

Deriving the local energy release rate from the J-integral of the cohesive crack, the jump terms vanish, while they persist for the matrix crack. Of course this feature is restricted to the chosen coordinate system x_1^*, x_2^*.

2.2. Matrix crack and interface center crack

The case of a cohesive center crack in an interface as illustrated in Fig. 1(b) is investigated next. Now there are two interface crack tips and therefore two cohesive zones, which will be referred to as α for the first and β for the second one. Eqs. (2) and (3) also apply to the case of Fig. 1(b), just the partition of the interface contours changes. With the depicted coordinate system x_1^*, x_2^* the J-integral vector of the matrix crack reads

$$\begin{aligned}J_k\vec{e}_k^* = &\left\{\lim_{\epsilon\to 0}\int_{\Gamma^+}(u^+ - u^-)n_k^+ \mathrm{d}\Gamma + \int_{\Gamma_A} Q_{kj}^A n_j \mathrm{d}\Gamma + \int_{\Gamma_B} Q_{kj}^B n_j \mathrm{d}\Gamma\right.\\ &\left. + \int_{\Gamma_{IB}^{closed}}(Q_{k2}^A - Q_{k2}^B)\mathrm{d}x_1^*\right\}\vec{e}_k^* + \int_{l_2}^{l_3}(u^A - u^B)\mathrm{d}x_1^*\vec{e}_2^*\\ &+ (J_{1,I}^{*coh\alpha} + J_{1,II}^{*coh\alpha} - J_{1,I}^{*coh\beta} - J_{1,II}^{*coh\beta})\vec{e}_1^*\\ &+ \frac{1}{2}\int_{\Gamma_{IB}^{coh}}[\sigma_{11}^A\varepsilon_{11}^A - \sigma_{11}^B\varepsilon_{11}^B + (\varepsilon_{22}^B - \varepsilon_{22}^A)\sigma_{22}]\mathrm{d}x_1^*\vec{e}_2^*.\end{aligned} \tag{13}$$

The $J_{1,I/II}^{*coh}$ have been introduced in Eq. (4) and are defined accordingly here. The terms in the second row of Eq. (13) comprise the sum of the loadings of the two cohesive crack tips. Separating Γ_{IB}^{coh} into the corresponding two parts yields

$$\begin{aligned}(J_k^\alpha + J_k^\beta)\vec{e}_k^* = &-(J_{1,I}^{*coh\alpha} + J_{1,II}^{*coh\alpha})\vec{e}_1^* + (J_{1,I}^{*coh\beta} + J_{1,II}^{*coh\beta})\vec{e}_1^*\\ &+ \frac{1}{2}\int_{l_1}^{l_2}[\sigma_{11}^B\varepsilon_{11}^B - \sigma_{11}^A\varepsilon_{11}^A + (\varepsilon_{22}^A - \varepsilon_{22}^B)\sigma_{22}]\mathrm{d}x_1^*\vec{e}_2^*\\ &+ \frac{1}{2}\int_{l_3}^{l_4}[\sigma_{11}^B\varepsilon_{11}^B - \sigma_{11}^A\varepsilon_{11}^A + (\varepsilon_{22}^A - \varepsilon_{22}^B)\sigma_{22}]\mathrm{d}x_1^*\vec{e}_2^*,\end{aligned} \tag{14}$$

whereat these terms are subtracted in Eq. (13). A closed integration contour $\Gamma_A + \Gamma_B$ around the cohesive center crack is obtained, closing the matrix crack, whereupon in a homogenous material ($A = B$) Eq. (14) and an integral along the cohesive crack surface $l_2 < x_1^* < l_3$ remain. Physically, the integral along $\Gamma_A + \Gamma_B$ then comprises the sum of the J-integrals of both cohesive crack tips and the configurational forces acting at the crack surfaces. For pure mode-I/II loadings the integral along $l_2 < x_1^* < l_3$ in Eq. (13) also vanishes just as the integral terms of $\vec{e}_2^*$ in Eq. (14) and the result thereof is $J_{1,I/II}^{*coh\beta} - J_{1,I/II}^{*coh\alpha}$.

The total energy release rate of the system is obtained as

$$\hat{G} = J_k z_k + J_k^\alpha z_k^\alpha + J_k^\beta z_k^\beta = \left(\lim_{\epsilon\to 0}\int_{\Gamma_\epsilon} Q_{kj}n_j \mathrm{d}\Gamma\right)z_k + \left(\lim_{\epsilon\to 0}\int_{\Gamma^\alpha} Q_{kj}n_j \mathrm{d}\Gamma\right)z_k^\alpha + \left(\lim_{\epsilon\to 0}\int_{\Gamma^\beta} Q_{kj}n_j \mathrm{d}\Gamma\right)z_k^\beta, \tag{15}$$

where the contour of the matrix crack is depicted in Fig. 1(b) and for the interface crack tips, counter clockwise integration contours shrunk to the cohesive surfaces are chosen. The global energy release rate is then calculated, inserting Eq. (13) into Eq. (15) with the interfacial crack growth vectors $z_k^\alpha \triangleq -\vec{e}_1^*$ and $z_k^\beta \triangleq \vec{e}_1^*$:

$$\begin{aligned}\hat{G} = &\left(\left\{\lim_{\epsilon\to 0}\int_{\Gamma^+}(u^+ - u^-)n_k^+ \mathrm{d}\Gamma + \int_{\Gamma_A} Q_{kj}^A n_j \mathrm{d}\Gamma + \int_{\Gamma_B} Q_{kj}^B n_j \mathrm{d}\Gamma\right.\right.\\ &\left.\left. + \int_{\Gamma_{IB}^{closed}}(Q_{k2}^A - Q_{k2}^B)\mathrm{d}\Gamma\right\}\vec{e}_k^* + \int_{l_2}^{l_3}(u^A - u^B)\mathrm{d}x_1^*\vec{e}_2^*\right.\\ &+ \frac{1}{2}\int_{\Gamma_{IB}^{coh}}[\sigma_{11}^A\varepsilon_{11}^A - \sigma_{11}^B\varepsilon_{11}^B + (\varepsilon_{22}^B - \varepsilon_{22}^A)\sigma_{22}]\mathrm{d}x_1^*\vec{e}_2^*\\ &+ (J_{1,I}^{*coh\alpha} + J_{1,II}^{*coh\alpha} - J_{1,I}^{*coh\beta} - J_{1,II}^{*coh\beta})\vec{e}_1^*)z_k\\ &+ G_I^{coh\alpha} + G_{II}^{coh\alpha} + G_I^{coh\beta} + G_{II}^{coh\beta}.\end{aligned} \tag{16}$$

Closing the matrix crack, loading the cohesive crack symmetrically and single mode and assuming equal traction separation laws for crack tips α and β, the J-integral of a contour $\Gamma_A + \Gamma_B$ vanishes, see Eq. (14), whereas the related energy release rates just vanish for a Yoffe type crack [14], i.e. $z_k^\alpha = z_k^\beta \triangleq \vec{e}_1^*$.

2.3. Matrix crack and crack in a self-contained interface

The case of a matrix crack in a bi-material body with a self-contained interface around material B and a remote integration contour is depicted in Fig. 1(c). In this case the formulation of the J-integral vector does not explicitly display the interface crack tip loading, i.e.

$$\begin{aligned}J_k &= \lim_{\epsilon\to 0}\int_{\Gamma_\epsilon} Q_{kj}n_j \mathrm{d}\Gamma\\ &= \lim_{\epsilon\to 0}\int_{\Gamma^+ + \Gamma^-} Q_{kj}n_j \mathrm{d}\Gamma + \int_{\Gamma_A} Q_{kj}n_j \mathrm{d}\Gamma + \int_{\Gamma_{IA}} Q_{kj}n_j \mathrm{d}\Gamma,\end{aligned} \tag{17}$$

however its influence is implicitly considered by the integrand of contour Γ_{IA}. The self-contained interface being excluded by Γ_{IA}, Eq. (17) is valid for perfect interfaces, holes or any kind of inclusion.

3. Imperfect interfaces and cohesive law

In contrast to perfect interfaces, where displacements and tractions t_i are continuous, weak or imperfect interfaces exhibit a jump of displacements in terms of separations δ_i. Interface cracks may thus occur [15], interacting with matrix cracks if present. Cohesive laws relate the cohesive tractions t_i and the separations δ_i. Assuming infinitesimal deformation and disregarding temperature changes or heat flux and also incorporating some spatial simplifications in the energy balance [16], yields the Clausius Duhem inequality according to [1]

$$\begin{aligned}0 &\leqslant -\dot{F}^{cz}(\delta_i, D_{ij}) + \dot{\delta}_i t_i\\ 0 &\leqslant \left[t_i - \frac{\partial F^{cz}(\delta_i, D_{ij})}{\partial \delta_i}\right]\dot{\delta}_i - \frac{\partial F^{cz}(\delta_i, D_{ij})}{\partial D_{ij}}\dot{D}_{ij}.\end{aligned} \tag{18}$$

The specific Helmholtz free energy F^{CZ} of a bilinear cohesive law is introduced as

$$F^{cz} = \frac{1}{2}\delta_i(\delta_{ij} - D_{ij})K_{jk}\delta_k, \tag{19}$$

where K_{jk} is the stiffness tensor and the matrix in which the scalar damage variables for the two loading modes are stored is the damage tensor D_{ij}:

$$\begin{aligned}K_{jk} &= \begin{bmatrix}K_{nn} & 0\\ 0 & K_{ss}\end{bmatrix};\\ D_{ij} &= \begin{bmatrix}A & 0\\ 0 & B\end{bmatrix} \quad \text{with} \quad A = \begin{cases}d_n & \forall\ d_s < 1\\ 1 & ,\, d_s = 1\end{cases} \quad \text{and} \quad B = \begin{cases}d_s & \forall\ d_n < 1\\ 1 & ,\, d_n = 1\end{cases}.\end{aligned} \tag{20}$$

The coupling of the damage evolution in normal and shear directions is neglected. The classical fracture mechanical crack opening modes are used to distinguish between a normal (mode I, normal to the

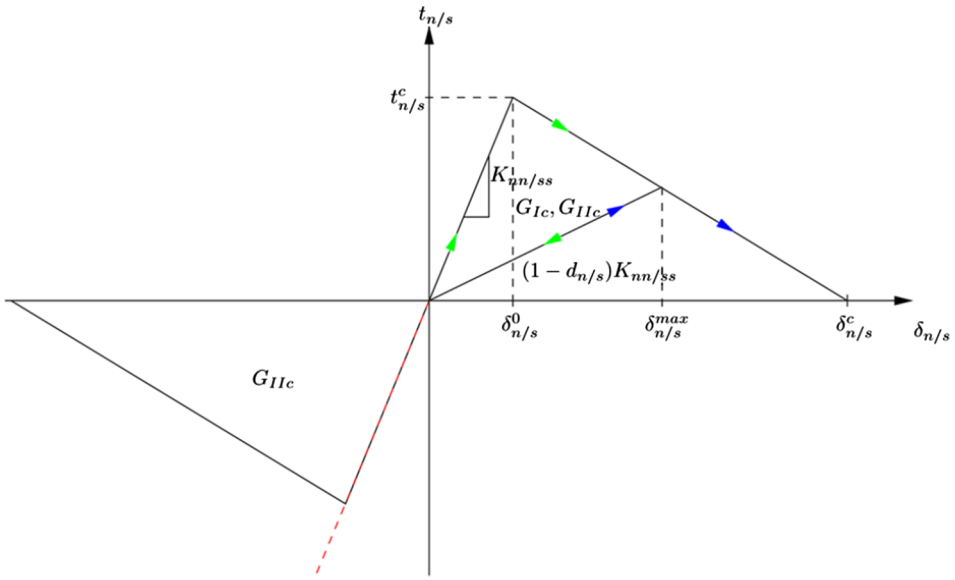

Fig. 2. Bilinear cohesive law for normal and shear (mode I/II) separation [1].

crack faces) and an in-plane shear (mode II, tangential to the crack faces) loading of the interface crack. The bilinear cohesive law depicted in Fig. 2 is derived from the partial derivative of the Helmholtz free energy with respect to the separation

$$t_i = \frac{\partial F^{cz}(\delta_i, D_{ij})}{\partial \delta_i} = (\delta_{ij} - D_{ij}) K_{jk} \delta_k, \tag{21}$$

with the critical energy release rates G_{Ic} and G_{IIc} of a virtual straight crack extension $z_k \triangleq \overrightarrow{e}_1^*$, according to Eq. (4) with $\delta_i^t = \delta_{ic}^t$ representing the areas underneath the curves for the two plane crack opening modes. For a negative separation, softening will not occur for normal loading, thus avoiding penetration and damage. For positive normal separation the same parameters are assumed as for shear separation. Inserting Eq. (21) into the dissipation inequality (18) yields

$$-\frac{\partial F^{cz}(\delta_i, D_{ij})}{\partial D_{ij}} \dot{D}_{ij} \geqslant 0. \tag{22}$$

With the specific Helmholtz free energy according to Eq. (19) the derivative reads

$$\frac{\partial F^{cz}(\delta_i, D_{ij})}{\partial D_{ij}} = -\frac{1}{2} \delta_i K_{jk} \delta_k, \tag{23}$$

so that the double scalar product of Eq. (22) finally provides the condition

$$\delta_1 K_{11} \delta_1 \dot{D}_{11} + \delta_2 K_{22} \delta_2 \dot{D}_{22} \geqslant 0, \tag{24}$$

revealing that the requirement for thermodynamic consistency is satisfied for positive stiffness and irreversible damage evolution, i.e. $\dot{D}_{ij} \geqslant 0$. The scalar damage variables d_n, d_s are calculated according to

$$d_{n/s} = \frac{\delta^c_{n/s}(\delta^{max}_{n/s} - \delta^0_{n/s})}{\delta^{max}_{n/s}(\delta^c_{n/s} - \delta^0_{n/s})}, \tag{25}$$

where $d_{n/s} \in [0, 1]$ and $\delta^{max}_{n/s}$ describes the maximum value of the separation for each crack opening mode attained during the loading history, see Fig. 2. In order to define the cohesive law, three independent parameters, e.g. $K_{nn/ss} = K$, $\delta^0_{n/s} = \delta^0$, and $G_{Ic/IIc} = G_c$ need to be set with the assumptions made. The other parameters are calculated as

$$t^c = K\delta^0; \quad \delta^c = \frac{2G_c}{t^c}. \tag{26}$$

4. Numerical examples of crack tip loading analysis and crack growth simulations

Numerical tools for the calculation of crack tip loading quantities based on the J-integral have been implemented into the commercial finite element code ABAQUS. Other approaches calculating the matrix crack tip loading, e.g. in terms of stress intensity factors (SIF), have not been employed since the J-integral in connection with large contours, thus not exploiting the inaccurate crack tip field, proved to be very accurate compared to most other methods of crack loading analysis [10]. A further advantage of calculating a J-integral vector instead of SIF is that it can directly be used to predict the direction of crack deflection. In order to investigate the effect of softening at a weak interface on the matrix crack tip loading, the model of Fig. 3 taken from [1] is investigated, with various cohesive laws listed in Table 1. Plane elastic structures are considered and while the introduced equations are also valid for bi-materials, single material structures with $E = 3039$ MPa, $\nu = 0.37$ and $K_{IC} = 32$ MPa$\sqrt{\text{mm}}$ are modelled in order to investigate the influence of the interface. The material parameters represent experimental data of an epoxy resin [17], where E is Young's modulus, ν Poission's ratio and K_{IC} is the fracture toughness which was assumed in the range of other epoxy resins as it has not yet been determined. An adaptive automatic stabilization scheme is applied in order to tackle the problem of numerical instability [18]. Results of the energy release rate of a matrix crack with the length $a_o = 15$ mm under displacement controlled loading conditions are shown in Fig. 3. The damage onset separation, the critical energy release rate and the critical traction are varied according to (a)-(c) in Table 1. Calculations with a perfect circular interface of radius $r = 7$ mm and also with a hole of equal size were performed for comparison. The results of [19] for straight bi-material interfaces already indicated that, even though energy is dissipated in the interface, the matrix crack tip loading can be larger than it would be for a perfect interface. These findings are confirmed for a circular imperfect interface in Fig. 3 (right), where the energy release rate is plotted versus the normalized displacement loading. The calculations for the imperfect interfaces result in significantly larger crack tip loadings than for a perfect interface as soon as damage occurs. As the toughness of the interface is reduced from (a) to (c), the most damage occurs for the cohesive law (c) where the matrix crack tip loading is the largest. The result of the perfect interface basically represents a lower bound of the energy release rate of the matrix crack. With increasing load displacement and thus cohesive crack

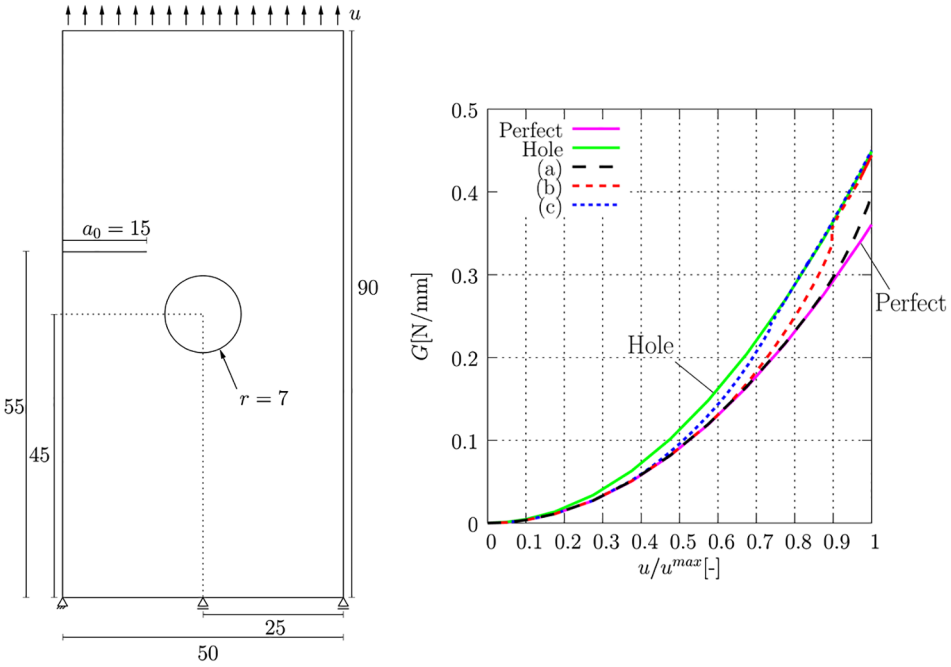

Fig. 3. Model for the crack tip loading analysis of an incipient matrix crack with length a_0 (size in mm, left) [1] and energy release rate plotted versus the normalized displacement loading (right): (a), (b), (c) from Table 1.

Table 1
Cohesive law parameters.

Cohesive parameters	K [N/mm^3]	δ^0 [mm]	G^c [N/mm]	t^c [MPa]	δ^c [mm]
(a)	10,000	0.0005	0.075	5	0.03
(b)	10,000	0.00035	0.0525	3.5	0.03
(c)	10,000	0.0002	0.03	2	0.03
(d)	100	0.5	20	50	0.8
(e)	1000	0.5	200	500	0.8
(f)	10,000	0.5	2000	5000	0.8
(g)	1000	0.005	2	5	0.8

growth the values abandon the lower limit, approaching those of the case of a hole. The latter at the first glance might appear to constitute an upper bound, however energy release rates for a delaminating interface may even exceed values of a hole. These results and those in [19] show that the loading of a matrix crack in the presence of an interface crack strongly depends on the alignment and shape of the crack and interface, as the matrix crack tip loading can decrease or increase even though energy is dissipated in the interface.

Crack growth simulations based on incremental extensions of the crack faces have been performed applying the same J-integral post-processor and the finite element code ABAQUS. The crack extensions

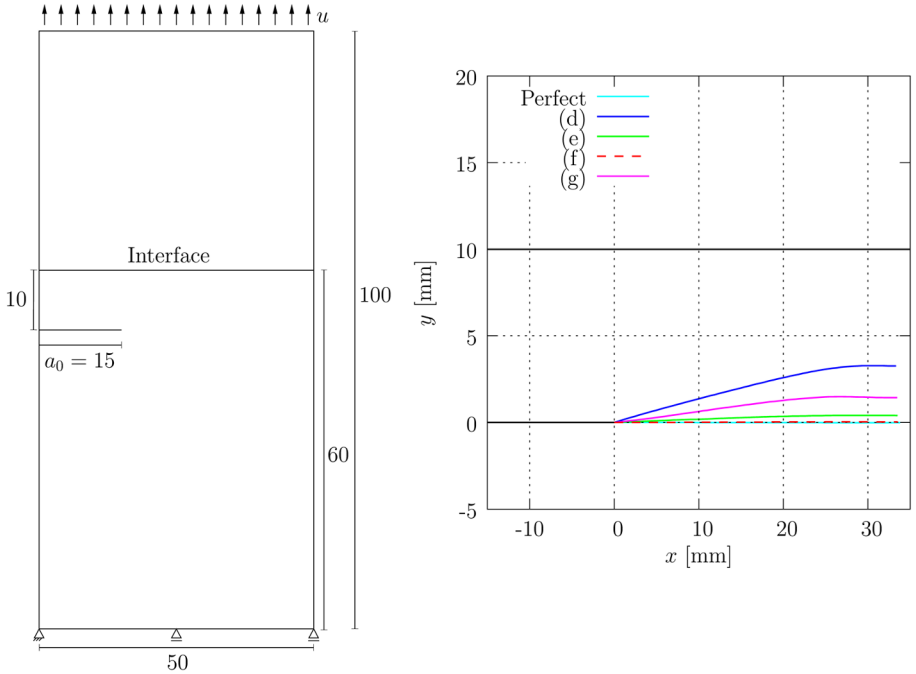

Fig. 4. Model with a straight interface for crack growth simulations (size in mm, left) and paths of the matrix crack with cohesive zones (d)–(g) from Table 1.

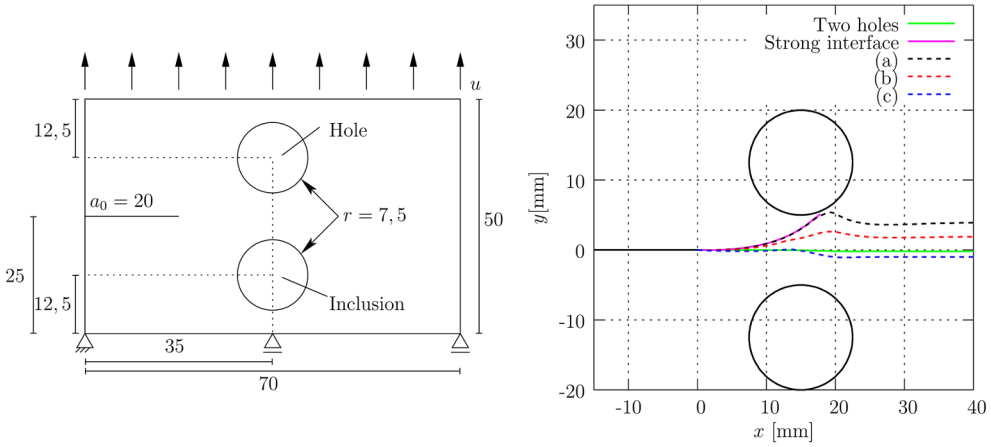

Fig. 5. Model with a hole and an inclusion bonded via an interface for crack path simulations (size in mm, left), and paths of the matrix crack with cohesive zones (a)–(c) from Table 1.

lead to repeated modifications of the geometry and therefore an intelligent re-meshing procedure is required [12,20]. The loading history cannot be neglected due to the dissipative processes in the cohesive zone and is stored in terms of the damage variables $d_{n/s}$. The energy release rate of the matrix crack is obtained as

$$G = J_k z_k. \tag{27}$$

A crack growth z_k in the direction of J_k thus maximizes the energy release rate and the reduction of total potential energy related to the area of virtual crack extension δA according to

$$\delta \Pi^{tot} = -J_k z_k \delta A. \tag{28}$$

This idea is postulated in the J-integral vector criterion of crack deflection [2], which will be applied in the following. With the prerequisite that mode I is the dominant loading mode, the J-integral provides accurate deflection angles. Other deflection criteria like the maximum circumferential stress criterion have been used as well for comparison, yielding identical crack paths.

The first model that is investigated is depicted in Fig. 4 (left). The crack in the model has an initial length of $a_0 = 15$ mm and a monotonically increasing displacement load u is applied, so that critical fracture conditions are represented in the crack growth simulations. With this model the influence of the interface stiffness K on the matrix crack growth is investigated, choosing the cohesive laws (d)-(g) depicted in Table 1. The stiffness is increased from (d)-(f) and δ^0 is chosen arbitrarily high, so that in the crack growth simulation $\delta_{n/s}^{max} < \delta^0$ holds and damage initiation is avoided. For the case of cohesive law (g), damage initiation is not prevented but a complete failure is avoided as $\delta^0 < \delta_{n/s}^{max} < \delta^c$ holds for the simulation. As a reference a matrix crack path is calculated for a perfect interface. The resulting crack paths are shown in Fig. 4 (right). The crack is not deflected with a perfect interface as it is subjected to mode I loading. For the stiffest interface (f) the crack is also not visibly deflecting. With lower stiffness a considerable deflection towards the interface is observed. Even though complete failure is avoided with cohesive law (g), the occurring damage is lowering the stiffness in parts of the interface, leading to an enlarged deflection in comparison to the case with the same stiffness but without damage ((e)). The choice of the interface stiffness depends on what the cohesive zone represents. For example if the interface is supposed to represent an adhesive layer, a finite stiffness is appropriate. Depending on the material, this layer might also attract a growing matrix crack, even though no damage occurs in it, shown by the results of Fig. 4. If the undamaged cohesive zone is not supposed to reduce the stiffness of the structure, the cohesive zone stiffness should be taken infinitely large [21] which, on the other hand, can cause numerical instability as soon as damage initiates. A reasonably large stiffness thus needs to be identified by trial and error. In Fig. 4 a reasonable value has been found with cohesive law (f), as the matrix crack is not deflected.

Another model with a hole and an inclusion is depicted in Fig. 5 (left), where the matrix crack has an initial length of $a_0 = 20$ mm. The inclusion and the matrix share the same material, except for one simulation where the inclusion also is modelled as a hole. If it is not the latter case, the interface is modelled perfect or imperfect with the cohesive laws (a)–(c) from Table 1. The undamaged interface stiffness almost reassembles a perfect interface concerning matrix crack deflection, shown by the results of Fig. 4. A monotonically increasing displacement load u is applied, so that critical fracture conditions are represented in the crack growth simulations. With this model the influence of interface damage and interface cracks, respectively, on a propagating matrix crack is investigated. The resulting crack paths, illustrated in Fig. 5 (right), are compared to a simulation with two holes and a simulation with a perfect interface. The damage onset separation, critical traction and energy release rate are reduced in the cohesive zone from law (a) to (c). Therefore more damage develops in the interface with cohesive law (c) than with cohesive law (a). For the case of two holes, the matrix crack does not deflect due to the symmetry of the model. The matrix crack grows into the hole if a perfect interface is considered, showing the preference of matrix cracks to grow into the direction of lower Young's modulus, being in good agreement with results from literature, e.g. [20,22,23]. Considering the weakest interface with cohesive law (c), the matrix crack is attracted by the damaged interface, even though a hole is present on the opposite side. Considering cohesive law (a), the matrix crack starts to follow the path of a perfect interface, indicating that no damage develops in the interface at the beginning. Almost grown into the hole, damage in the interface develops at larger displacement load. This prevents the matrix crack from growing into the hole but deflects it towards the inclusion, eventually growing to the outer boundary. The matrix crack path for cohesive law (b), being in between the paths for laws (a) and (c), is in accordance with the cohesive law parameters of (b), being in between those of laws (a) and (c).

5. Conclusion

In this work the J-integral vector is calculated for a matrix crack tip using remote integration contours including an interface crack, so that the path independence requires extensions. The additional constituents are investigated to provide physical interpretations. One part of the formulation is a generalization of the scalar J-integral for cohesive zones derived by Rice [3], now providing a J-integral vector, describing the interface crack tip loading and its influence on the loading of the matrix crack and thus on its deflection.

One advantage of applying the J-integral as fracture mechanical loading quantity is that crack deflection and crack paths are straightforwardly predicted in the present examples, not requiring additional consideration, e.g. of hoop stress. Furthermore, the line integral implementation proves to provide very accurate results with comparatively low computational cost.

Matrix crack tip loading analysis in the presence of a weak interface is performed, showing that the energy release rate not necessarily decreases due to energy dissipation in the cohesive zone. Matrix crack paths are simulated for structures with a straight interface, investigating the influence of the initial interface stiffness. For sufficiently low stiffness, a matrix crack tends to grow towards the interface. When damage occurs, the deflecting effect is amplified. The significant influence of delamination on a propagating matrix crack is shown in a model with a hole and with an inclusion bonded by an interface, providing two competing attractive effects on a growing matrix crack. The matrix crack grows towards the hole without interface damage, however with increasing delamination the matrix crack tends to grow towards the interface.

Acknowledgements

Financial support by the DFG is gratefully acknowledged.

References

[1] J. Scheel, A. Ricoeur, Weak and strong bi-material interfaces and their influence on propagating cracks in plane elastic structures, Proc. Struct. Integrity 5 (2017) 255–262.
[2] H.C. Strifors, A generalized force measure of conditions at crack tips, Int. J. Solids Struct. 10 (1974) 1389–1404.
[3] J.R. Rice, A path independent integral and the approximate analysis of strain concentration by notches and cracks, J. Appl. Mech. 35 (1968) 379–386.
[4] G.P. Cherepanov, Crack propagation in continuous media (translation from russian), J. Appl. Math. Mech. 31 (3) (1967) 503–512.
[5] J.D. Eshelby, The continuum theory of lattice defects, Solid State Phys. 3 (1956) 79–144.
[6] G.I. Barenblatt, Mathematical theory of equilibrium cracks in brittle fracture, Adv. Appl. Mech. 7 (1962) 55–129.
[7] B. Budiansky, J.R. Rice, Conservation laws and energy-release rates, J. Appl. Mech. 40 (1973) 201–203.
[8] R.E. Smelser, M.E. Gurtin, On the J-integral for bi-material bodies, Int. J. Fract. 13 (1977) 382–384.
[9] R. Khandelwal, C.J.M. Kishen, Complex variable method of computing for bi-material interface cracks, Eng. Fract. Mech. 73 (2006) 1568–1580.
[10] M. Kuna, Finite Elements in Fracture Mechanics vol. 10, Springer, Dordrecht, 2013.
[11] J.W. Eischen, An improved method for computing the integral, Eng. Fract. Mech. 26 (1987) 697–700.
[12] P.O. Judt, A. Ricoeur, Accurate loading analyses of curved cracks under mixed-mode conditions applying the J-integral, Int. J. Fract. 182 (2013) 53–66.
[13] P.O. Judt, A. Ricoeur, Crack growth simulation of multiple cracks systems applying remote contour interaction integrals, Theor. Appl. Fract. Mec. 75 (2015) 78–88.
[14] E.H. Yoffe, LXXV The moving Griffith crack, Phil. Mag. 42 (1951) 739–750.
[15] Z. Hashin, Thin interphase/imperfect interface in elasticity with application to coated fiber composites, J. Mech. Phys. Solids 50 (2002) 2509–2537.
[16] N.S. Ottosen, M. Ristinmaa, J. Mosler, Fundamental physical principles and cohesive zone models at finite displacements – limitations and possibilities, Int. J. Solids Struct. 53 (2015) 70–79.
[17] M. Kahlmeyer, A. Winkel, J. Scheel, I. Melnyk, A. Müller, A. Fery, A. Ricoeur, S. Böhm, Microencapsulated markers for damage detection in adhesive joints, J. Adhes. 94 (10) (2018) 767–783.
[18] N. N., Abaqus 6.11 Online Documentation/Abaqus Analysis User's Manual, Dassault Systèmes, 2011.
[19] P. Judt, A. Ricoeur, Numerical investigations in structures with imperfect material interfaces and cracks, Proc. Appl. Math. Mech. 16 (2016) 143–144.
[20] P.O. Judt, A. Ricoeur, G. Linek, Crack path prediction in rolled aluminum plates with fracture toughness orthotropy and experimental validation, Eng. Fract. Mech. 138 (2015) 33–48.
[21] V. Tomar, J. Zhai, M. Zhou, Bounds for element size in a variable stiffness cohesive finite element model, Int. J. Numer. Meth. Eng. 61 (2004) 1894–1920.
[22] M. Kikuchi, Y. Wada, Y. Li, Crack growth simulation in heterogeneous material by S-FEM, Eng. Fract. Mech. 167 (2016) 239–247.
[23] M.T. Tilbrook, K. Rozenburg, E.D. Steffler, L. Rutgers, M. Hoffman, Crack propagation paths in layered, graded composites, Compos. Part B – Eng. 37 (2006) 490–498.